AIMS Materials Science, 12(4): 845–860.
DOI: 10.3934/matersci.2025036
Received: 12 May 2025
Revised: 30 July 2025
Accepted: 12 August 2025
Published: 28 August 2025

https://www.aimspress.com/journal/Materials

Research article

Coating-assisted laser micromachining of UHMWPE: Thermal control and microchannel optimisation using PDMS and PAA

Ojo Kurdi[1], Eko Hadi[2,*], Ari Santosa[2], Muhammad Hadi[2], Rifky Ismail[1] and Oktarina Heriyani[3]

[1] Department of Mechanical Engineering, Faculty of Engineering, Diponegoro University, Jl. Prof Sudharto, Tembalang, Semarang, Central Java 50275, Indonesia
[2] Department of Naval Architecture, Faculty of Engineering, Diponegoro University, Jl. Prof Sudharto, Tembalang, Semarang, Central Java 50275, Indonesia
[3] Department of Mechanical Engineering, Faculty of Industrial and Informatics Technology, Muhammadiyah University, Prof. Dr. HAMKA, Jakarta Timur 13830, DKI Jakarta, Indonesia

* **Correspondence:** Email: ekosasmito@ft.undip.ac.id; Tel: +62-819-012-80458.

Abstract: Ultra-high molecular weight polyethylene (UHMWPE) is established as a material of choice in tribological and biomedical applications because of its superior impact resilience, low coefficient of friction, and outstanding wear resistance. Nevertheless, its intrinsic low thermal conductivity poses significant challenges during laser surface texture (LST), manifesting as thermal anomalies, including surface bulging and geometric distortion. In this study, we addressed these limitations by implementing a thermal regulation framework that integrates polymeric coatings, polyacrylic acid (PAA) and polydimethylsiloxane (PDMS), to mitigate thermally induced deformation in diode laser micromachining. A uniform coating thickness of 150 µm was applied through a controlled screen-printing protocol. The samples were then textured using a 520 nm, 4 W diode laser in a matrix of focal distances (22 to 54 mm) and scanning speeds (2 to 10 mm/s). Quantitative characterization of the resulting microchannels was conducted using confocal microscopy and profilometry, emphasizing dimensional metrics such as depth, width, and height of the curve. PDMS-coated substrates consistently demonstrated superior thermal stability and geometric accuracy among all configurations. At the optimal settings identified (38 mm focal distance, 4 mm/s scanning speed), microchannels exhibited a depth of 43.2 µm, a width of 35.2 µm and a minimal bulge height of 10 µm. This investigation contributes a scalable and cost-efficient approach to the advancing laser-based micromachining of UHMWPE, particularly in applications requiring precise surface architectures. The demonstrated integration of laser parameter optimization with polymer-based thermal modulation offers significant

implications for designing and fabricating high-performance components in seawater-lubricated tribosystems and microfluidic biomedical platforms.

Keywords: UHMWPE; laser texturing; PDMS coating; thermal damage; microchannels; tribology

1. Introduction

Ultra-high molecular weight polyethylene (UHMWPE) has emerged as a strategic material in biomedical and marine engineering due to its exceptional wear resistance, intrinsic lubricity, chemical inertness, and low friction coefficient; characteristics that ensure its functional integrity under corrosive, high-load operating conditions [1]. Its negligible water uptake and long-term chemical stability make it highly suitable for tribological applications involving seawater exposure, with its performance further enhanced through nano- and micro-scale reinforcement strategies employing graphene oxide or ceramic fillers [2,3]. Despite these merits, UHMWPE's performance can be compromised under abrasive aquatic conditions and elevated thermal loading, resulting in wear-induced surface fatigue and molecular chain degradation [4–6]. These constraints require continuous innovation in surface modification, material reinforcement, and lubrication frameworks to increase the reliability of UHMWPE-based systems [7,8].

Among modification techniques, laser surface texturing (LST) has gained prominence for producing engineered surface morphologies such as microgrooves and dimples, which serve to reduce contact area, trap lubricants, and improve hydrodynamic performance [7]. Compared to conventional machining, LST offers superior control over feature geometry, energy efficiency, and environmental sustainability [9,10]. Empirical studies have demonstrated significant frictional reductions, up to 50%, with optimized texture geometries, particularly rectangular and square patterns under aqueous lubrication [8,11]. However, UHMWPE's inherently low thermal conductivity and high melt viscosity present challenges during laser processing, such as bulging, irregular ablation profiles, and thermal degradation that hinder precise feature fabrication [9,10,12].

Attempts to mitigate these effects using thermal buffers such as metal foils or coolant sprays have had limited success [10]. In contrast, polymer-based coatings like polyacrylic acid (PAA) and polydimethylsiloxane (PDMS) offer promising alternatives due to their favorable thermal properties, specifically, moderate conductivities and high boiling points, and their demonstrated efficacy in reducing surface bulging under sub-6 W laser regim42es [13–15]. These materials act as transient thermal barriers, modulating the laser-induced heat flux reaching the substrate and stabilizing the resulting surface topography [10].

Building on this foundation, we expand upon previous work [10]. We systematically investigate how focal distance (22–54 mm) and scanning speed (2–10 mm/s) interact with coating type to affect microstructural outcomes in LST of UHMWPE. While other researchers have focused mainly on laser power or ambient conditions, we interrogate the synergistic influence of coating-substrate dynamics and beam positioning parameters. The insights derived provide a refined processing window for high-fidelity surface texture of UHMWPE components, especially for marine tribosystems and biocompatible fluidic devices [15–17].

From an application standpoint, UHMWPE's role in the marine and biomedical sectors is multifaceted. In marine systems, its high-strength fibres are deployed in mooring cables, anchor lines,

and underwater ropes, where its lightweight profile and wear resistance outperform steel-based analogs [18–20]. Its self-lubricating nature and chemical robustness make it ideal for submerged bearings and wear-resistant bushings [1]. Moreover, in biomedical engineering, UHMWPE is indispensable in orthopedic implants and surgical sutures due to its long-term biocompatibility and mechanical endurance [21–23]. Bio functional modifications enhance their utility for controlled drug delivery and cell adhesion in implantable systems.

UHMWPE remains superior to other thermoplastics for load bearing tribological and biomedical applications due to its excellent fatigue resistance, ultra-low wear rate, and high tensile strength. These properties render it particularly advantageous in joint replacements and sliding interfaces against metallic counterparts [24,25]. In addition, UHMWPE's oxidative stability and structural retention under cyclic loading make it robust against degradation mechanisms that affect other polymers [25]. Reinforcement with nanomaterials or bioactive agents has further improved its wear and mechanical profiles [25], demonstrating scalability in clinical and industrial applications [26].

Nevertheless, its thermal and structural limitations remain a critical bottleneck during laser exposure. At high temperatures, UHMWPE undergoes a phase transition due to molecular chain mobility exceeding crystalline cohesion, resulting in softening, dimensional instability, and degradation of load-bearing properties [27,28]. Prolonged thermal exposure leads to chain scission and reduced molecular weight, further compromising its functional life [16]. Moreover, localized overheating during laser ablation can weaken interfacial bonds and reduce the efficacy of surface reinforcements [29,30].

Recent advances in LST have introduced ultrashort pulsed lasers (e.g., femtosecond and picosecond) to mitigate thermal artifacts. These lasers produce confined energy deposition via nonlinear photon absorption, thereby enabling precise material removal with negligible heat-affected zones (HAZ) [31]. "Cold ablation" phenomena enable the structuring of UHMWPE without inducing thermal degradation, rendering such methods ideal for polymer substrates sensitive to thermal diffusion [32,33]. Putignano et al. (2019) further validated this approach by demonstrating significant friction reduction, up to 60%, on soft matter substrates using femtosecond lasers to fabricate micro dimples that preserved surface integrity while enhancing hydrodynamic lubrication [34].

Although we employ nanosecond laser sources, the discussion acknowledges the technical superiority of ultrafast lasers and situates the current work within a practical and scalable fabrication context. The choice of nanosecond lasers was primarily dictated by equipment accessibility and cost-efficiency, which aligns with industrial constraints [35]. Hybrid approaches, such as post-texture chemical etching or integrated magnetic actuation, have also been explored to alleviate thermal residuals and improve microchannel fidelity [36–38]. These strategies complement the coating-based approach investigated here, reinforcing the objective of achieving high-precision, thermally stable surface architectures in polymeric systems.

In sum, we advance the understanding of how functional coatings interact with laser parameters to modulate thermal behavior and geometry fidelity in UHMWPE micromachining. Integrating controlled coating deposition and process optimization presents a robust pathway for translating laboratory-scale innovations into industrially viable surface engineering solutions across marine and biomedical domains.

2. Materials and methods

2.1. Materials

The experimental work entailed UHMWPE substrates procured from Henan Sanyou Plastic Engineering Development Co., Ltd., due to their documented mechanical robustness, including high wear resistance and impact resilience; critical parameters for thermomechanical stability in laser-assisted surface engineering [39]. The samples were dimensioned at 50 × 100 × 5 mm with initial surface roughness ranging from 0.20 to 0.25 ± 0.04 μm. Black pigmentation was selected to improve contrast during post-ablation optical and profilometric imaging [10]. Thermophysical attributes such as a melting point of 132 to 138 °C and a tensile strength between 39 and 48 MPa underscore the relevance of the polymer for the miniaturization of biomedical and tribological devices [40,41]. These properties are summarized in Table 1. UHMWPE samples were coated with PAA and PDMS to attenuate thermally induced distortions during laser micromachining. The coatings were uniformly applied using a controlled screen-printing method to a target thickness of 150 μm [10]. Unlike other studies that lacked procedural transparency, we utilized a 100 mesh/inch stainless steel screen and a semi-automated flatbed printer. The coating gels were spread with a 75 Shore-A squeegee at room temperature (25 °C), and the samples were air-cured for 30 min before subsequent laser exposure [32]. The coating characteristics relevant to heat dissipation and optical modulation are defined in Table 2.

Table 1. Thermomechanical properties of UHMWPE relevant to laser micromachining [34,40,42].

Property	Value
Melting temperature (°C)	132–138
Molecular weight (10^6 g/mol)	3.5–7.5
Specific gravity	0.925–0.945
Poisson's ratio	0.46
Modulus of elasticity (GPa)	0.5–0.8
Tensile ultimate strength (MPa)	39–48
Tensile yield strength (MPa)	21–28
Tensile ultimate elongation (%)	350–525
Degree of crystallinity (%)	39–75
Impact strength (J/m of notch)	1070

Table 2. Physical parameters of PAA and PDMS coatings for thermal shielding [13–15].

Property	PAA	PDMS
Density	1.09 g/cm^3 (30% aq.)	0.97 kg/m^3
Thermal conductivity (W/m·K)	0.37	0.15
Boiling point (°C)	116	155–220
Melting point (°C)	106	~–40
Index of refraction	1.442	1.4

2.2. Experimental setup

Laser surface modification was conducted using a 520 nm diode laser (Sharp OPT-A-B20000) operating at 4-Watt power, 20 kHz pulse frequency, and 130 ns pulse duration [10]. The beam scanning was performed using Sanyo Denki stepper motors (35HSH24140-18), coordinated by an Arduino Uno Rev 3 microcontroller for spatial precision. Three processing conditions were investigated: uncoated (air), PAA-coated, and PDMS-coated UHMWPE. Each coating maintained a uniform 150 μm thickness. The metric variations included focal distances (22, 30, 38, 46, and 54 mm) and scanning velocities (2, 4, 6, 8, and 10 mm/s) to elucidate the dynamics of beam-material interaction [9,12,43]. The experimental configurations are tabulated in Table 3.

Table 3. Laser micromachining parameters and process settings [10].

Process parameter	Value
Focal standard (mm)	38
Focal distances (mm)	22, 30, 38, 46, 54
Laser average power (W)	4
Laser pulse frequency (kHz)	20
Laser pulse duration (ns)	130
Laser traverse speed (mm/s)	2, 4, 6, 8, 10
Processing environment	Air, PDMS liquid gel, PAA liquid gel
Liquid gel thickness (μm)	150

2.3. Procedure

The procedural workflow encompassed five sequential phases, illustrated in Figure 1:

(a) Preparation of samples

UHMWPE sheets were precisely cut to 50 × 100 × 5 mm dimensions. The surfaces were thoroughly cleaned to ensure consistent topographic conditions, achieving a surface roughness of 0.2 to 0.25 μm as measured before coating application.

(b) Coating application

To protect the polymer surface from thermal degradation during laser ablation, two types of liquid gel coatings, PAA and PDMS, were applied using a screen-printing technique. Each layer was deposited at a uniform thickness of 150 μm. These materials were selected for their known thermal buffering and optical modulation properties [13,14].

(c) Laser texturing

A diode laser system (520 nm) was used to perform surface texture by engraving rectangular microchannels under various focal distances and scanning speeds, as detailed in Table 3. With this process, we aimed to improve surface characteristics, such as wettability and tribological performance of UHMWPE in marine environments [8,40,44,45].

(d) Cleaning

The samples were cleaned using an ultrasonic bath filled with distilled water for 10 min after laser processing. This step was necessary to remove residual gel, ablation by-products, and loose particulates from the microstructure surface.

(e) Surface analysis

The resulting microchannel geometries were characterized using a confocal microscope (Am Scope ME300TZB-2L-9M). Quantitative analysis of channel depth, width, and bulge formation was conducted using Gwyddion and ImageJ software, following standardized 3D profilometric methods [10].

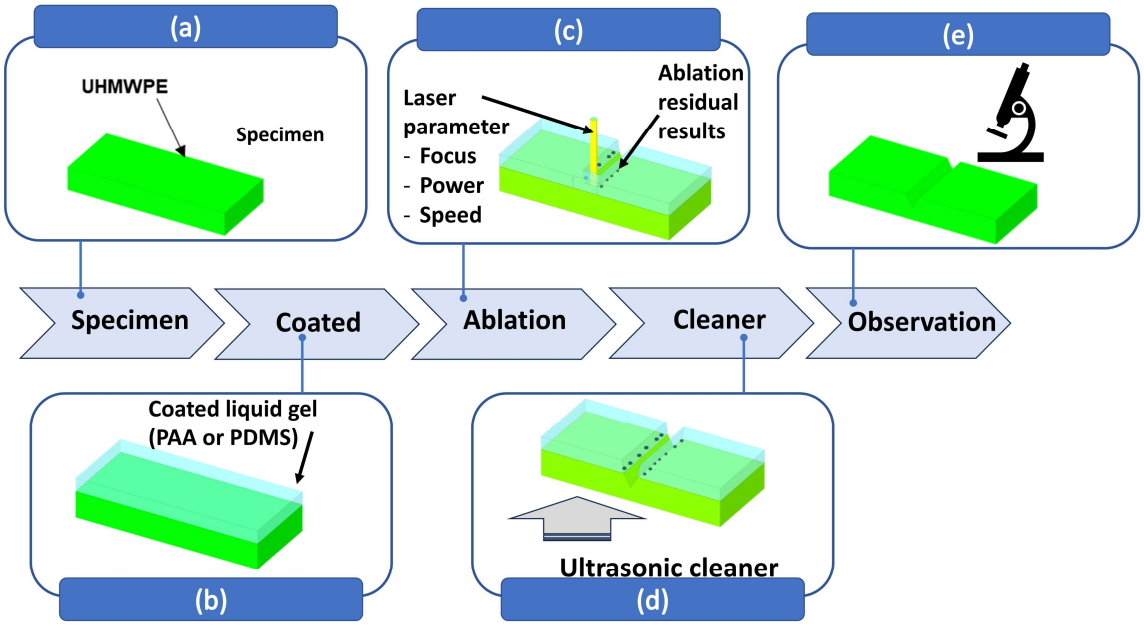

Figure 1. Experimental flow chart adapted from Hadi et al. [10]. (a) Selection and preparation of samples; (b) coating deposition via screen printing; (c) laser micromachining in varied settings; (d) ultrasonic post-processing; (e) confocal and profilometric evaluation.

2.4. Data analysis

Dimensional analysis was performed by reconstructing 3D surface topographies using Gwyddion while ImageJ facilitated 2D cross-sectional quantification. The channel depth, width, and bulge metrics were extracted under varying coating and laser parameters. Statistical assessments, including variance analysis, delineated the thermal suppression efficacy of PAA and PDMS coatings. Researchers have verified that such coatings significantly improve feature integrity and ablation uniformity under pulsed laser exposure [12,44].

3. Results and discussion

3.1. Influence of focal distance on microchannel fidelity and thermal deformation

The impact of focal distance variation (22, 30, 38, 46, and 54 mm) was investigated under constant laser power (4 watts) and scan velocity (4 mm/s) to quantify its role in microchannel definition and thermal response of PDMS-coated UHMWPE substrates. The optimal focal setting of 38 mm produced the most refined microchannels, achieving a depth of 43.2 μm and a width of 35.2 μm, validated by confocal microscopy [10].

Significant deterioration in ablation performance was observed at suboptimal distances (22 and 54 mm), including depth reductions to 18.8 µm and width expansions up to 53.7 µm, indicating dilution of the energy density due to beam defocusing. These effects were consistent with previous findings that associate off-focus laser processing with expanded heat-affected zones and inefficient material removal [38,46–49].

Uncoated UHMWPE exhibited pronounced thermal bulging, particularly at a focal distance of 22 mm, due to unmitigated lateral heat dissipation. In contrast, PDMS-coated specimens consistently exhibited minimal bulge formation, underscoring the coating's ability to buffer thermal energy through its high boiling point and low optical refractive index [14–17], as demonstrated in Figure 2a–c.

Figures 2d–e provides a quantitative overview, affirming that PDMS coatings produce narrower, shallower, and geometrically consistent channels when combined with optimal focal settings. This evidence shows the synergistic effect of beam parameter control and thermally protective coatings in enhancing micromachining outcomes.

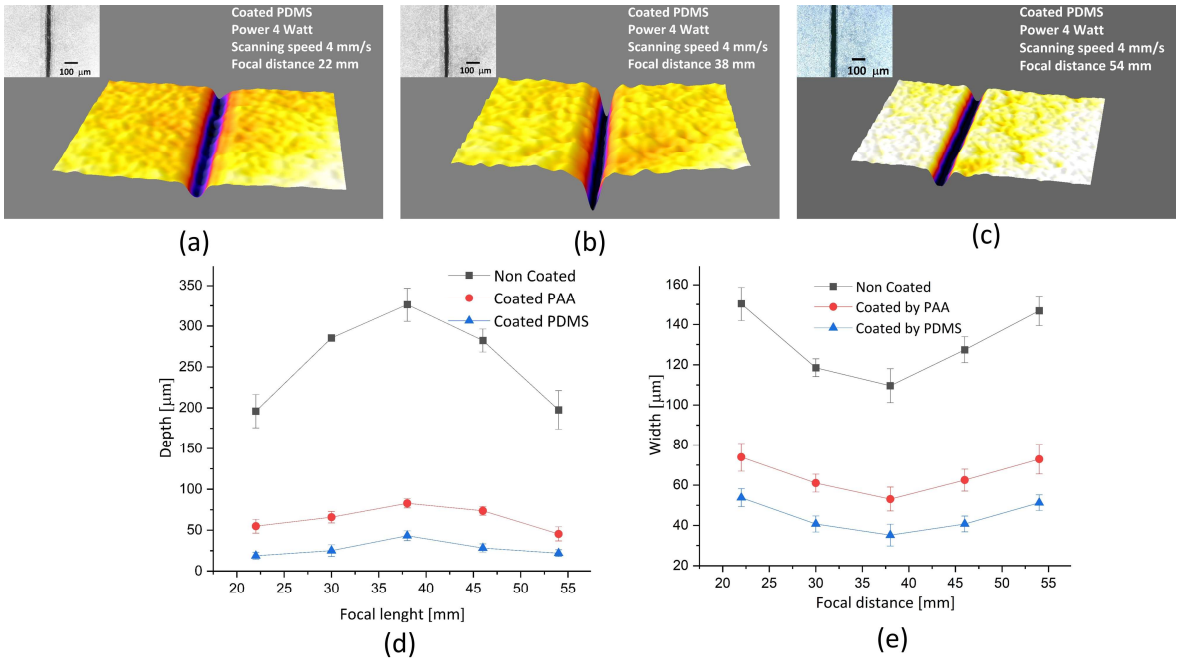

Figure 2. Effect of focal distance on microchannel morphology. (a–c) Confocal imaging of UHMWPE coated with PDMS at 22, 38, and 54 mm; (d) channel depth vs. focal distance; and (e) channel width vs. focal distance under three coating regimes.

3.2. Role of scanning speed in ablation dynamics and heat-induced defects

A range of scanning speeds (2 to 10 mm/s) was assessed under fixed laser power (4 watts) and optimal focal length (38 mm). Slower scan rates led to increased ablation depths because of longer energy-material interaction. For example, uncoated UHMWPE at 2 mm/s reached 293 µm depth, while 10 mm/s yielded 216 µm [10]. However, extended thermal exposure at slower speeds also exacerbated bulging, reaching heights of up to 45 µm [36,37].

As illustrated in Figure 3a–c, the PDMS-coated samples showed smoother profiles and reduced deformation at all speeds. Quantitative trends in Figure 3d–f revealed that PDMS coatings not only

limited the maximum bulge height to 25 µm (vs. 45 µm uncoated) but also moderated the depth of the channel, improving the dimensional stability [10].

The insulating characteristics of PDMS outperform the more thermally conductive PAA, enabling enhanced thermal management during high-energy input [45,50]. These results corroborate prior studies indicating that while slower speeds increase material removal efficiency, they heighten thermal stress unless mediated by protective coatings [17,37,47,51].

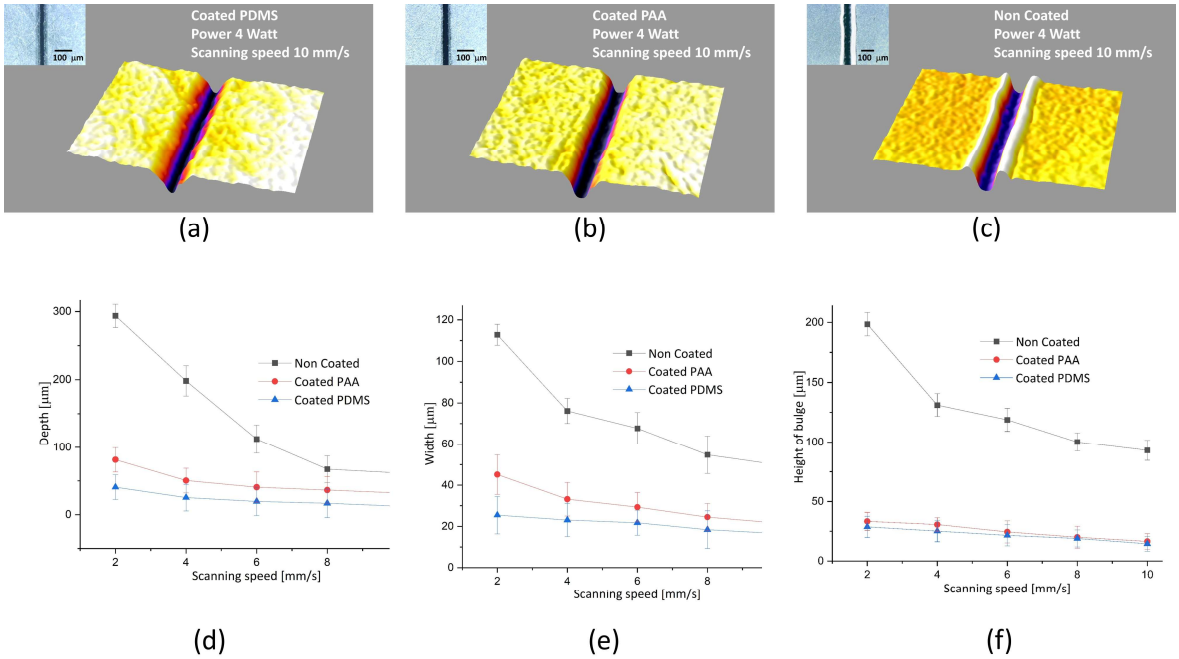

Figure 3. Effect of focal distance on microchannel morphology. (a–c) Confocal imaging of UHMWPE coated with PDMS, PAA and non-coated at 38 mm; (d) channel depth vs. scanning speed; (e) channel width vs. scanning speed; and (f) height of bulge vs. scanning speed.

3.3. Functional implications for tribologically relevant applications

The 38 mm focal distance and scanning speeds between 4 and 6 mm/s produced microchannels optimized for lubricant retention and minimal thermal deformation. These geometries, including channels of 43.2 µm depth and 35.2 µm width, are critical for reducing friction and improving fluid film stability in seawater-lubricated bearing systems [52,53]. Hydrophilic contributions from PAA coatings further improve lubrication performance via hydration-layer formation, promoting shear adaptability [53].

Performance metrics detailed in Table 4 underscore the superiority of PDMS in both optimal and non-optimal settings. PDMS coating reduced bulging by 80% compared to uncoated controls. Under unfavorable parameters (22 mm focal, 2 mm/s speed), PDMS still constrained bulge height to 130 µm instead of 195 µm for uncoated surfaces.

Table 4. Comparative microchannel geometries for UHMWPE substrate under various coating and parameter conditions.

Condition	Coating	Channel depth (μm)	Channel width (μm)	Bulge height (μm)
Optimal	Uncoated	160	79	130
Optimal	PAA-coated	60	36	35
Optimal	PDMS-coated	31	22	25
Non-optimal	Uncoated	293	112	195
Non-optimal	PAA-coated	80	45	39
Non-optimal	PDMS-coated	45	22	30

These geometries facilitate robust fluid film retention and enhance load-carrying capability under dynamic lubrication, echoing results from studies on microtopography-induced tribological improvements [1,54]. PDMS's superior thermal insulation also preserves surface fidelity, which is vital for long-term performance in aqueous or saline conditions [1,50].

The demonstrated effectiveness of PDMS in suppressing deformation while enhancing channel fidelity has broader implications for biomedical micromachining. In such contexts, precision and reproducibility of microchannel dimensions are essential for reliable implant functionality. PDMS's favorable thermal and optical properties thus make it a compelling candidate for precision polymer micromachining in high-stakes applications [8,38].

3.4. Mechanistic insights into coating–laser interactions

The physicochemical interplay between the PDMS and PAA coatings and the incident laser field determines the surface morphology and thermally induced microstructural evolution. Due to its inherent thermal resilience and elasticity, PDMS supports the generation of hierarchical nanostructures via localized laser-induced phase transitions. These structures enhance surface functionality by improving wetting dynamics and surface adhesion; properties critical to microfluidics and biosensor integration [50,55]. In contrast, PAA demonstrates superior electrochemical interfacial characteristics, facilitating charge redistribution and stronger substrate bonding, essential for applications demanding interfacial robustness [36].

Thermodynamically, PDMS moderates heat flux through low thermal conductivity and elevated thermal decomposition thresholds, thereby acting as an efficient thermal buffer. This limits heat penetration into the UHMWPE matrix and curtails lateral heat dissipation, resulting in minimized bulge formation. In contrast, PAA, despite its higher thermal conductivity, accelerates heat transfer to the substrate, increasing the risk of surface deformation under similar processing conditions.

3.5. Functional implications of microchannel geometries

The tribological efficacy of laser-textured UHMWPE surfaces is intrinsically linked to the dimensional configuration of the fabricated microchannels. The depth and width govern the lubricant reservoir capacity and shear-flow dynamics, which influence the formation and sustainability of hydrodynamic films. Empirical studies underscore that deeper channels increase fluid retention, thereby improving film longevity and suppressing wear mechanisms under dynamic load [8,52,53].

Modulation of the aspect ratio provides additional control over interfacial shear stress and pressure gradients. Although higher ratios promote effective load distribution and lubricant shearing, excessive channel widths can disrupt laminar flow, induce cavitation, and compromise lubrication efficacy [38,47,48]. Therefore, optimized geometries enabled by PDMS-based micromachining exhibit high structural fidelity and align with tribological demands for prolonged operational reliability.

3.6. Thermal field management via scanning speed and focal control

Heat-affected zone (HAZ) minimization remains a critical target in laser micromachining of thermally sensitive polymers. The temporal dimension of the beam-material interaction, dictated by scanning speed, is inversely correlated with heat accumulation. High scanning velocities reduce the thermal load per unit area, narrowing the HAZ and preserving the morphology of the substrate [17,38,47,48,56,57]. In contrast, slow speeds extend the duration of exposure, facilitating deeper ablation but exacerbating residual thermal effects.

The focal distance, a determinant of the energy flux density at the target interface, directly affects precision and collateral damage. Reduced focal lengths intensify beam convergence, achieving finer ablation profiles and constrained thermal propagation. Extended focal distances dilute the energy density, increasing lateral thermal diffusion and expanding HAZ [38]. The concurrent optimization of these parameters is imperative for achieving reproducible, damage-free micro-structuring in UHMWPE substrates.

3.7. Thermo-optical mechanisms governing bulge suppression

Bulge formation, a prevalent thermal defect in polymer micromachining, arises from re-solidified melt flow and differential thermal contraction. In PDMS, high-temperature decomposition than melting initiates localized material ablation, releasing volatile fragments that dissipate heat and inhibit volumetric expansion [17,37,47,50,57]. This phenomenon results in reduced mechanical distortion and enhanced dimensional retention.

From an optical perspective, PDMS exhibits favorable absorption characteristics and a refractive index conducive to efficient photothermal conversion. These attributes support precise photon-material interactions with minimized collateral energy diffusion. Optimization of laser wavelength selection, pulse duration, and focus further refines energy localization and suppresses thermomechanical damage [17,38,47,48].

3.8. Coating-driven thermal damage mitigation models

The application of surface coatings for thermal regulation is grounded in thermophysical energy absorption and dissipation models. Coatings with tailored emissivity and conductivity parameters intercept and redistribute laser energy, preventing excessive substrate heating and subsequent polymer degradation. This thermal buffering mechanism is particularly effective in regulating near-surface temperature gradients during high-flux laser exposure.

Remelting and reflow phenomena after deposition contribute to the densification and homogenization of the coating layers, sealing micro voids, and inhibiting the localized heat concentration [17,37,47,57]. Although previously cited mechanisms involving antimony trioxide and multilayer optics lacked

empirical substantiation, current validated approaches affirm that optimized single-layer coatings with consistent thermal response profiles ensure uniform ablation and structural integrity.

Collectively, these thermo-optical mechanisms reinforce the utility of engineered coatings in advancing the precision and reproducibility of polymer laser micromachining. Strategic material selection and processing control yield robust and functionally adaptive microstructures suited for demanding engineering and biomedical contexts.

4. Conclusions

This investigation substantiates the critical role of surface coatings, specifically PAA and PDMS, in enhancing the fidelity and functional integrity of laser micromachined UHMWPE. Both coatings act as modulators of interfacial thermal dynamics, mitigating adverse effects such as bulge formation, irregular channel geometry, and thermal degradation intrinsic to UHMWPE's low thermal conductivity. Among the two, PDMS exhibited superior thermal regulation performance, due to its low thermal conductivity and high decomposition threshold, which enabled precise microchannel fabrication with minimal dimensional deviation.

Experimental optimization identified a focal distance of 38 mm and a scanning speed of 4 mm/s as optimal processing parameters. Under these conditions, the PDMS-coated samples produced microchannels characterized by a minimal bulge height, reduced lateral expansion, and a well-defined depth. These geometric characteristics are essential for tribological applications, where surface uniformity governs lubricant entrainment, friction modulation, and wear resistance.

In addition to thermal modulation, the PDMS coatings facilitated enhanced photon-material coupling, yielding improved ablation precision and preserving substrate morphology. This dual thermal and optical functionality advantage makes PDMS an ideal candidate for high-precision engineering tasks. In biomedical contexts, the ability of PDMS to support the formation of smooth microchannels with a high-aspect-ratio with minimal collateral damage is particularly advantageous for applications in implantable systems and microfluidic architectures.

In sum, we establish that laser micromachining of UHMWPE can be significantly advanced through an integrated strategy combining optimized beam parameters and functional coating technologies. In the future, researchers should investigate the interactive effects of coating thickness, pulse duration, repetition frequency, and multi-pass strategies to refine microstructural outcomes. Furthermore, utilizing PDMS or comparable thermally robust coatings in emerging tribological and biomedical platforms may yield advances in surface engineering precision, functionality, and application scalability.

Use of AI tools declaration

The authors declare they have not used Artificial Intelligence (AI) tools in the creation of this article.

Acknowledgments

This research was funded by the Directorate of Research and Community Service, Deputy Director of Strengthening Research and Development, Ministry of Research and Technology/National Research and Innovation Agency of Indonesia, under the 2021 fiscal year grant (No. 8/E1/KPT/2021),

with Contract Number: 187-34/UN7.6.1/PP2021. The authors also sincerely thank the Materials Laboratory, Department of Naval Architecture, Faculty of Engineering, Diponegoro University, for providing experimental facilities and technical support throughout this study.

Author contributions

Ojo Kurdi: conceptualization, writing; Eko Hadi: writing—original draft, editing, validation; Ari Santosa: formal analysis; Muhammad Hadi: visualization; Oktarina Heriyani: data curation, investigation; Rifky Ismail: supervision, review.

Conflict of interest

The authors declare no conflict of interest.

References

1. Cheng B, Shang H, Duan H, et al. (2025) Tribological behavior of ultra-high molecular weight polyethylene (UHMWPE) with different molecular weights under artificial seawater lubrication. *J Appl Polym Sci* 142: e56918. https://doi.org/10.1002/app.56918
2. Zhou X, Li B, Huang Q, et al. (2025) Effects of graphene oxide and graphene spatial orientation on tribological properties of UHMWPE composites. *Wear* 564–565: 205684. https://doi.org/10.1016/j.wear.2024.205684
3. Hussain O, Ahmad B, Sheikh SS (2021) Biotribological performance of medical-grade UHMW polyethylene-based hybrid composite for joint replacement. *Polym Polym Compos* 29: S1424–S1431. https://doi.org/10.1177/09673911211058088
4. Li W, Wang Z, Liu N, et al. (2022) Study on tribological characteristics of ultra-high molecular weight polyethylene under unsaturated lubrication of water and brine. *Polymers* 14: 4138. https://doi.org/10.3390/polym14194138
5. Chang T, Yuan C, Guo Z (2019) Tribological behavior of aged UHMWPE under water-lubricated condition. *Tribol Int* 133: 1–11. https://doi.org/10.1016/j.triboint.2018.12.038
6. Baena JC, Peng Z (2017) Mechanical and tribological performance of UHMWPE influenced by temperature change. *Polym Test* 62: 102–109. https://doi.org/10.1016/j.polymertesting.2017.06.017
7. Rahman MDM, Biswas MAS, Hoque KN (2022) Recent development on micro-texturing of UHMWPE surfaces for orthopedic bearings: A review. *Biotribology* 31: 100216. https://doi.org/10.1016/j.biotri.2022.100216
8. Sufyan M, Hussain M, Ahmad H, et al. (2019) Bulge micro-textures influence on tribological performance of ultra-high-molecular-weight-polyethylene (UHMWPE) under phosphatidylcholine (lipid) and bovine serum albumin (BSA) solutions. *Biomed Phys Eng Express* 5: 035021. https://doi.org/10.1088/2057-1976/ab0e94
9. Cheng B, Shang H, Duan H, et al.(2024) Influence of laser-induced surface carbonization on the tribological properties of UHMWPE in a seawater environment. *Appl Surf Sci* 645: 158873. https://doi.org/10.1016/j.apsusc.2023.158873

10. Hadi ES, Kurdi O, BS AW, et al. (2022) Influence of laser processing conditions for the manufacture of microchannels on ultrahigh molecular weight polyethylene coated with PDMS and PAA. *AIMS Mater Sci* 9: 554–571. https://doi.org/10.3934/matersci.2022033
11. López-Cervantes A, Domínguez-López I, Barceinas-Sánchez JDO, et al. (2013) Effects of surface texturing on the performance of biocompatible UHMWPE as a bearing material during in vitro lubricated sliding/rolling motion. *J Mech Behav Biomed Mater* 20: 45–53. https://doi.org/10.1016/j.jmbbm.2012.12.010
12. Hussain M, Sufyan M, Abbas N, et al. (2019) Influence of laser processing conditions for texturing on ultra-high-molecular-weight-polyethylene (UHMWPE) surface. *Case Stud Therm Eng* 14: 100491. https://doi.org/10.1016/j.csite.2019.100491
13. Yang X, Shi M, Dong L, et al. (2010) Effect of UV irradiation on mechanical properties and structure of poly(1,3,4-oxadiazole) fibers. *Polym Degrad Stab* 95: 2467–2473. https://doi.org/10.1016/j.polymdegradstab.2010.08.006
14. Zhu Y, Jiang Y, Lin R, et al. (2017) Research on thermal degradation process of p-nitrophenol-based polybenzoxazine. *Polym Degrad Stab* 141: 1–10. https://doi.org/10.1016/j.polymdegradstab.2017.05.001
15. McDonald JC, Whitesides GM (2002) Poly(dimethylsiloxane) as a material for fabricating microfluidic devices. *Acc Chem Res* 35: 491–499. https://doi.org/10.1021/ar010110q
16. Skakov M, Ocheredko I, Tuyakbayev B, et al. (2023) Development and studying of the technology for thermal spraying of coatings made from ultra-high-molecular-weight polyethylene. *Coatings* 13: 698. https://doi.org/10.3390/coatings13040698
17. Wang C, Bai X, Guo Z, et al. (2021) Friction and wear behaviours of polyacrylamide hydrogel microsphere/UHMWPE composite under water lubrication. *Wear* 477: 203841. https://doi.org/10.1016/j.wear.2021.203841
18. Sheng C, He G, Hu Z, et al. (2021) Yarn on yarn abrasion failure mechanism of ultrahigh molecular weight polyethylene fiber. *J Eng Fiber Fabr* 16: 1–9. https://doi.org/10.1177/15589250211052766
19. Asik MD, Walsh-Rock E, Inverardi N, et al. (2025) Enhanced antibiotic release and mechanical strength in UHMWPE antibiotic blends. *J Bone Joint Surg* 107: 586–593. https://doi.org/10.2106/JBJS.24.00689
20. Hussain M, Naqvi RA, Abbas N, et al. (2020) Ultra-high-molecular-weight-polyethylene (UHMWPE) as a promising polymer material for biomedical applications: A concise review. *Polymers* 12: 323. https://doi.org/10.3390/polym12020323
21. Sobajima A, Okihara T, Moriyama S, et al. (2020) Multiwall carbon nanotube composites as artificial joint materials. *ACS Biomater Sci Eng* 6: 7032–7040. https://doi.org/10.1021/acsbiomaterials.0c00916
22. Zhang X, Tan D, Tang Q, et al. (2024) Impact of thermo-oxidative aging on the dry tribological performance and wear mechanisms of UHMWPE/ZrO_2 friction pairs. *AIP Adv* 14: 035143. https://doi.org/10.1063/5.0197569
23. Singh DK, Verma RK (2021) A critical review on ultra high molecular weight polyethylene (UHMWPE) for prosthesis and implant functions. *E3S Web Conf* 309: 01018. https://doi.org/10.1051/e3sconf/202130901018

24. AL-Maatoq M, Fuentealba P, Fachet M, et al. (2022) Carbon nanotube-based reinforced polymers for medical applications: Improving impact strength of polymer-polymer composites. *J Nanomater* 2022: 1760198. https://doi.org/10.1155/2022/1760198
25. Singh S, Das A, Kumar N, et al. (2025) Study on cut-resistance properties of composite yarn-based knitted UHMWPE textiles: Influence of reinforcement, radiant heat exposure, outdoor environment, and cutting angles. *J Appl Polym Sci* 142: e56690. https://doi.org/10.1002/app.56690
26. Khalil Y, Hopkinson N, Kowalski AJ, et al. (2022) Investigating the feasibility of processing activated carbon/UHMWPE polymer composite using laser powder bed fusion. *Polymers* 14: 3320. https://doi.org/10.3390/polym14163320
27. Wang M, Zhang Y, Bin J, et al. (2022) Cold laser micro-machining of PDMS as an encapsulation layer for soft implantable neural interface. *Micromachines* 13: 1484. https://doi.org/10.3390/mi13091484
28. Nayak C, Balani K (2021) Effects of reinforcements and gamma-irradiation on wear performance of ultra-high molecular weight polyethylene as acetabular cup liner in hip-joint arthroplasty: A review. *J Appl Polym Sci* 138: e51275. https://doi.org/10.1002/app.51275
29. Zhang Y, Jiang Q, Long M, et al. (2022) Femtosecond laser-induced periodic structures: Mechanisms, techniques, and applications. *Opto-Electron Sci* 1: 220005. https://doi.org/10.29026/oes.2022.220005
30. Ham SS, Lee H (2020) Development of method enhanced laser ablation efficiency according to fine curvature of the polymer through the preliminary preparation process using UV picosecond laser. *Polymers* 12: 959. https://doi.org/10.3390/polym12040959
31. Paknejad M, Azarhoushang B, Zahedi A, et al. (2022) Investigation of material removal mechanisms of laser-structured Si_3N_4 via single diamond grit scratching. *Res Sq*. https://doi.org/10.21203/rs.3.rs-1974605/v1
32. Putignano C, Scarati D, Gaudiuso C, et al. (2019) Soft matter laser micro-texturing for friction reduction: An experimental investigation. *Tribol Int* 136: 82–86. https://doi.org/10.1016/j.triboint.2019.03.001
33. Faruk O, Yang Y, Zhang J, et al. (2023) A comprehensive review of ultrahigh molecular weight polyethylene fibers for applications based on their different preparation techniques. *Adv Polym Technol* 2023: 6656692. https://doi.org/10.1155/2023/6656692
34. Rudnik E, Dobkowski Z (1997) Thermal degradation of UHMWPE. *J Therm Anal* 49: 471–475. https://doi.org/10.1007/BF01987473
35. Lei C, Pan Z, Chen J, et al. (2018) Influence of processing parameters on the structure size of microchannel processed by femtosecond laser. *Opt Laser Technol* 106: 47–51. https://doi.org/10.1016/j.optlastec.2018.03.024
36. Cai T, Zhan S, Yang T, et al. (2022) Study on the tribological properties of UHMWPE modified by UV-induced grafting under seawater lubrication. *Tribol Int* 168: 107419. https://doi.org/10.1016/j.triboint.2021.107419
37. Vadivel HS, Somberg J, Kalin M, et al. (2022) Tribological performance of a UHMWPE-based multiscale composite under different lubrication and loads. *Lubr Sci* 34: 480–492. https://doi.org/10.1002/ls.1603
38. Imran M, Rahman RA, Ahmad M, et al. (2016) Fabrication of microchannels on PMMA using a low-power CO_2 laser. *Laser Phys* 26: 096101. https://doi.org/10.1088/1054-660X/26/9/096101

39. Fernández-Pradas JM, Naranjo-León S, Morenza JL, et al. (2012) Surface modification of UHMWPE with infrared femtosecond laser. *Appl Surf Sci* 258: 9256–9259. https://doi.org/10.1016/j.apsusc.2011.09.106
40. Konari PR, Clayton YD, Vaughan MB, et al. (2021) Experimental analysis of laser micromachining of microchannels in common microfluidic substrates. *Micromachines* 12: 1–13. https://doi.org/10.3390/mi12020138
41. Teixidor D, Orozco F, Thepsonthi T, et al. (2013) Effect of process parameters in nanosecond pulsed laser micromachining of PMMA-based microchannels at near-infrared and ultraviolet wavelengths. *Int J Adv Manuf Technol* 67: 1651–1664. https://doi.org/10.1007/s00170-012-4598-x
42. Adrian M, Zaharescu T, Jipa S, et al. (2008) The assessment of thermal and radiation stability of UHMWPE. *J Optoelectron Adv Mater* 10: 826–829.
43. Darvishi S, Cubaud T, Longtin JP (2012) Ultrafast laser machining of tapered microchannels in glass and PDMS. *Opt Lasers Eng* 50: 210–214. https://doi.org/10.1016/j.optlaseng.2011.09.003
44. Chung CK, Lin SL, Wang HY, et al. (2013) Fabrication and simulation of glass micromachining using CO_2 laser processing with PDMS protection. *Appl Phys A* 113: 501–507. https://doi.org/10.1007/s00339-013-7555-0
45. Chung CK, Lin YC, Huang GR (2005) Bulge formation and improvement of the polymer in CO_2 laser micromachining. *J Micromech Microeng* 15: 1878–1884. https://doi.org/10.1088/0960-1317/15/10/013
46. Zhang D, Chen A, Wang Q, et al. (2020) Influence of distance between sample surface and focal point on the expansion dynamics of laser-induced silicon plasma under different sample temperatures in air. *Optik* 202: 163511. https://doi.org/10.1016/j.ijleo.2019.163511
47. Gu L, Yu G, Li CW (2018) A fast and low-cost microfabrication approach for six types of thermoplastic substrates with reduced feature size and minimized bulges using sacrificial layer-assisted laser engraving. *Anal Chim Acta* 997: 24–34. https://doi.org/10.1016/j.aca.2017.10.030
48. Sunderlal Singh S, Khare A, Joshi SN (2020) Fabrication of microchannel on polycarbonate below the laser ablation threshold by repeated scan via the second harmonic of Q-switched Nd:YAG laser. *J Manuf Process* 55: 359–372. https://doi.org/10.1016/j.jmapro.2020.04.006
49. Zhao R, Ma C, Gao X, et al. (2023) Investigation of overflow-water-assisted femtosecond laser-induced plasma modulation of microchannel morphology. *Coatings* 13: 1541. https://doi.org/10.3390/coatings13091541
50. Ariati R, Sales F, Souza A, et al. (2021) Polydimethylsiloxane composites characterization and its applications: A review. *Polymers* 13: 4258. https://doi.org/10.3390/polym13234258
51. Ndeda R (2012) Modeling of factors influencing bulge formation in polymers during laser micromachining.
52. Feng H, Jiang S, Shang-Guan Y (2021) Three-dimensional computational fluid dynamic analysis of high-speed water-lubricated hydrodynamic journal bearing with groove texture considering turbulence. *Proc Inst Mech Eng Part J* 235: 2272–2286. https://doi.org/10.1177/1350650121998519
53. Cai J, Han Y, Xiang G, et al. (2022) Influence of the mass conservation cavitation boundary on the tribo-dynamic responses of the micro-groove water-lubricated bearing. *Surf Topogr Metrol Prop* 10: 045011. https://doi.org/10.1088/2051-672X/ac9acd

54. Kunizhev BI, Torshkhoeva ZS, Zhelikhazhev RN, et al. (2021) Destruction of polymers under the action of laser radiation. *IOP Conf Ser Mater Sci Eng* 1083: 012040. https://doi.org/10.1088/1757-899X/1083/1/012040
55. Chakraborty A, Gottumukkala NR, Gupta MC (2023) Superhydrophobic surface by laser ablation of PDMS. *Langmuir* 39: 11259–11267. https://doi.org/10.1021/acs.langmuir.3c00818
56. Fan J, Jiang S, Liu Y, et al. (2025) Advanced porous SiO_x/PAA microarchitectures: A sustainable approach to high-capacity and ultra-stable anodes. *ACS Appl Mater Interfaces* 17: 29669–29680. https://doi.org/10.1021/acsami.5c03534
57. Liang X, Yang Z (2021) Experimental study on the influence of friction pair material hardness on the tribological behaviors of water-lubricated thrust bearings. *Ind Lubr Tribol* 73: 929–936. https://doi.org/10.1108/ilt-03-2021-0083

AIMS Press